International Research Journal of Multidisciplinary Scope (IRJMS), 2025; 6(2): 930-940

Original Article | ISSN (O): 2582-631X DOI: 10.47857/irjms.2025.v06i02.03634

A Hybrid Inception Network for Hyperspectral Imaging-based Bloodstain Classification

Tejaskumar B Sheth[1]*, Milind S Shah[2], Suhas H Patel[1]

[1]Electronics and Communication Department, Government Engineering College, Gandhinagar-382028, Gujarat, India, [2]Electronics and Communication Department, SSEC, Bhavnagar-364001, Gujarat, India. *Corresponding Author's Email: tbsheth@gmail.com

Abstract

In forensic science, blood is a crucial piece of evidence for reconstructing crime scenes. Identifying and classifying blood can help confirm a suspect's involvement, though various chemical processes are employed to identify bloodstains at the crime scene. However, such processes may deteriorate the obtained material and interfere with further DNA analysis. Hyperspectral Imaging (HSI) is a promising noncontact technique that can be utilized in forensic science examination at crime scenes for body fluid classification, including bloodstain detection and classification. Therefore, this work demonstrates the use of Hybrid Inception networks for HSI data analysis for bloodstain recognition and classification. For testing and validation, we make use of a Hyperspectral-based Bloodstain dataset that is openly accessible. A variety of detection scenarios with differing degrees of complexity are incorporated in this dataset. It allows evaluation of how well machine learning techniques work in various backgrounds, acquisition environments, blood ages, and situations where additional blood-like compounds are present. We conducted blood detection experiments using this dataset. We use the proposed Hybrid Inception network to compare the findings against a variety of widely accessible cutting-edge deep learning models, including 3D CNN, Hybrid CNN, and the Inception model. We carefully evaluate the results and discuss each examined architecture, taking into consideration the limited supply of training samples. Experiments show that the modified Inception network is an efficient and accurate classification model.

Keywords: Bloodstain Classification, Crime Scene Investigation, Deep Learning, Spectral Information, Hyperspectral Imaging, Inception Network.

Introduction

Body fluid identification, such as "blood" identification, is important in violent crime cases because it can give key evidence in a criminal investigation and help the court reach a decision. Establishing a link between identifying the fluid or tissue and the DNA profile strengthens this proof. Numerous chemical techniques are employed for identifying and analysing blood evidence, which can help confirm a suspect's involvement in a crime (1). These traditional chemical-based methods, while effective, can negatively impact future DNA analysis, which is crucial for conclusive identification. DNA analysis itself is both time-consuming and expensive, requiring significant resources. Additionally, the risk of false positives, such as mistaking a dark paint stain for blood, can lead to considerable waste of time and effort, diverting attention and resources from more accurate lines of investigation. This underscores the need for more reliable and less invasive methods to analyse and classify blood evidence at crime scenes.

Tests like Leucomalachite Green (LMG), Benzidine, and Luminol are commonly used to identify bloodstains. These tests work by causing a colour change when the reagent reacts with the blood, indicating its presence (2). However, the use of chemicals and the preparation of samples are often involved in these methods, which can complicate further investigations, such as pattern analysis and DNA testing. The evidence can be altered or degraded by the chemicals, potentially leading to the destruction of its original context and making future forensic analysis more difficult. Due to these limitations, non-destructive methods for identifying recent evidence are increasingly being sought by forensic investigators. Various spectroscopic methods, including Raman spectroscopy, Reflectance spectroscopy, Electron Paramagnetic Resonance (EPR), Nuclear Magnetic

(Received 27th December 2024; Accepted 14th April 2025; Published 30th April 2025)

Resonance (NMR), and Infrared (IR) spectroscopy —particularly Attenuated Total Reflectance Fourier Transform Infrared (ATR-FTIR) spectroscopy—have demonstrated potential in detecting bloodstains at crime scenes (3). While these spectroscopic techniques offer high sensitivity and specificity for bloodstain identification, they also require significant expertise and laboratory analysis. Proper interpretation of the spectroscopic data necessitates specialized knowledge and experience. Additionally, the equipment used for these analyses can be sophisticated and expensive, making them less accessible for routine crime scene investigations. However, their ability to produce non-destructive and extremely precise results makes them essential instruments in forensic science, potentially improving the accuracy and speed of bloodstain identification and analysis at crime scenes. The spectral characteristics of blood components, particularly haemoglobin, make HSI a powerful tool for identifying and analysing bloodstains. Blood consists of approximately 45% cellular elements, including red and white blood cells and platelets, with haemoglobin as the primary component of red blood cells. In a healthy individual, haemoglobin exists in two main forms: deoxyhaemoglobin (deoxyHb) and oxyhaemoglobin (oxyHb). Without biological processes to maintain its state, oxyHb undergoes oxidation to form methaemoglobin (metHb), which further degrades into hemichrome (HC). OxyHb exhibits distinct spectral features, including absorption dips in the reflectance spectrum near 414nm (*Soret* band) and at approximately 542nm and 576nm (α and β bands) (4). The progressive degradation of oxyHb to metHb over time is reflected in spectral variations at these wavelengths. HSI captures the unique spectral signatures of oxyHb and metHb, providing detailed spectral and spatial data crucial for the accurate classification of human bloodstains at crime scenes.

A significant concern is how different substances behave in HSI with diverse spatial and spectral properties, such as those obtained at crime scene, particularly under the deceptive visual background. A publicly available HSI dataset was utilized in this study, in which each scenario features a section of a prepared mock-up crime scene containing background materials of various colors, shapes, and compositions (5). Blood traces of various sizes and shapes are strategically placed within the scene alongside visually similar substances, such as artificial blood, tomato juice, and red paint. As a result, the complexity of the detection task varies across scenarios, ranging from simple settings with a uniform white background to more challenging environments with diverse backgrounds and multiple blood-like substances.

Deep learning techniques for HSIC have shown promising outcomes in recent years. As a result, one of the best ways to extract more detailed spatial, spectral, or spatiospectral feature information in HSIC has been found to be CNN-based approaches. Specifically, state-of-the-art performance in the field of HSI classification has been demonstrated by supervised convolutional neural networks (CNNs) and their variations—including 1D-CNNs, 2D-CNNs, 3D-CNNs, and HybridCNN—through the successful extraction of deep spectral-spatial information (6).

CNN-based methods are increasingly being adopted due to their effectiveness in enhancing classification performance. In HSI classification, 2D CNNs are commonly used to extract spatial features, while 3D CNNs capture spatial-spectral information simultaneously. To improve these approaches, a hybrid CNN model was introduced that integrates multiscale spatial-spectral features using a combination of 3D and 2D CNNs (7). Similarly, a hybrid spectral CNN (HybridSN) was developed for hyperspectral remote sensing image classification, leveraging both 3D and 2D CNNs (8). In this model, 3D CNNs extract spatial-spectral features from stacked spectral bands, followed by 2D CNNs to refine spatial feature extraction. Additionally, an Inception-inspired architecture was proposed, incorporating 3D and 2D Inception blocks to enhance spatial-spectral feature learning (9).

Deep learning models' performance is largely dependent on the amount of training samples. However, labelling hyperspectral data is challenging and time-consuming, resulting in a shortage of annotate freely available dataset. Limited training data can lead to effective model overfitting, which means they perform well on training data but poorly on new and unknown data (10). To address these inherent challenges, we proposed a modified Inception network based on the Google Inception architecture for HSI classification (11).

To identify blood at crime scenes, forensic scientists use a variety of chemical approaches. The Kastle-Meyer (KM) test, for example, is a popular presumptive test that uses the interaction of phenolphthalein and hemoglobin to generate a pink colour, suggesting the presence of blood. This test is highly sensitive, identifying blood at a dilution ratio of one in 10,000 (12). However, its sensitivity can result in false positives when reacting with compounds such as rust or specific plants. Another approach, the Leucomalachite Green (LMG) test, detects blood at comparable dilution levels and creates a green colour. While some studies suggest that LMG is as sensitive as KM, others claim it is less effective and, like KM, can produce false positives with certain compounds (13).

The luminol test is another popular procedure recognized for its ability to identify blood traces that are invisible to the human eye. When sprayed on a suspicious region, luminol interacts with the iron in haemoglobin, giving off a blue glow in the dark. This makes it particularly beneficial for spotting clean or faint bloodstains. However, luminol's efficiency is limited by its need for darkness and its ability to react with other chemicals including some metals, bleach, and plant materials, resulting in false positives. Furthermore, the chemical reaction might dilute or erase DNA evidence, complicating future forensic investigations. Despite these disadvantages, luminol's great sensitivity and ability to detect buried blood traces make it an important tool in crime scene investigations (14).

Various spectroscopic techniques are employed for bloodstain analysis, each with unique benefits and limitations. Near-Infrared (NIR) spectroscopy is non-destructive and suitable for dried samples, offering high accuracy in bloodstain identification when paired with pattern recognition techniques (15). However, sophisticated calibration is required. Raman spectroscopy provides a detailed molecular fingerprint, making it highly specific and effective for complex mixtures, though its accuracy decreases for dried samples due to blood structure degradation by powered laser light (16). Fourier Transform Infrared (FTIR) spectroscopy offers detailed molecular information and can differentiate between human and non-human species, gender, and age groups, but it faces challenges with overlapping spectral features and precise sample preparation (17). Vibrational spectroscopy, which integrates IR absorption and Raman scattering, offers detailed blood identification and age estimation but is complex and resource intensive. Electron Paramagnetic Resonance (EPR) spectroscopy detects unpaired electrons in blood components but demands specialized equipment (18).

HSI offers significant advantages for bloodstain classification over chemical and traditional spectroscopic methods. It is a non-destructive method that protects the integrity of the evidence by obtaining precise spectral information for every pixel over a broad range of wavelengths, improving the ability to distinguish blood from other substances. Using both spatial and spectral mapping, HSI facilitates sophisticated multivariate analysis and increases the precision of crime scene reconstructions. It permits real-time, in situ analysis without requiring much sample preparation like various spectroscopic methods and lowers false positives that are frequently encountered in chemical procedures (19). The development of deep learning architectures for HSI classification in the field of forensic science has grown substantially in recent years.

A detailed evaluation of deep learning architectures for bloodstain classification was presented, including recurrent neural networks (RNNs), multilayer perceptron (MLPs), and 1D, 2D, and 3D CNNs. Taking Support Vector Machine (SVM) as a baseline, it was found that 3D CNNs and RNNs performed better than conventional models, emphasising the importance of customising neural networks for hyperspectral data (20). Since deep learning often requires extensive labelled data, the development of architectures aimed at reducing this dependency has been considered encouraging. Notably, a hybrid CNN with a bit short training datasets was used to examine classification accuracy. To compare the suggested models, the Hybrid CNN architecture was also used as a baseline in this study. However, due to the limited amount of training data, a tendency toward overfitting was observed in these models (21).

This study proposes a novel approach that integrates a 3D/2D CNN Inception module with a Hybrid Inception-based 3D/2D CNN architecture.

The hybrid Inception module is designed to enhance both depth and width within the network by incorporating 3D and 2D convolutional layers alongside 3D and 2D max-pooling layers. In essence, the Inception module applies multiple convolutional and max-pooling layers simultaneously to the same input, with the outputs subsequently concatenated. This multi-branch structure enables efficient multi-scale feature extraction, allowing the network to capture diverse spatial-spectral information. By leveraging multiple convolutional layers, the proposed method enhances feature representation and improves overall classification performance. The following summarises the contributions of the work.

- Proposed Hybrid Inception architecture shows the improvement in HIS classification with adopting convolution kernel size with incremental filter size.
- The use of 3D CNN with 2D CNN as hybrid structure shows increase in performance when spectral and special parameter consider for HIS classification.
- The proposed approach demonstrates its utility in forensic science as a non-destructive, effective, and quick tool for identifying bloodstains.

The paper is structured as follows: after reviewing related forensic HSI studies, the subsequent sections detail the implemented methodology, present the dataset and results, and conclude with directions for future research.

Methodology

HSI is a technique that collects and analyses data across the electromagnetic spectrum, with each pixel containing spectral information that enables accurate material identification. The hyperspectral cube $s \epsilon \mathcal{R}^{(M \times N \times L)}$ represents data with spatial dimensions M and N, and spectral dimension L. This comprehensive data format is ideal for detailed analysis and classification tasks.

As each pixel in HIS has number of spectral band (typically 100+) this high-dimensional data requires significant computational resources and time. As the number of dimensions grows, the feature space expands rapidly, making it harder for the model to learn and generalize. Principal Component Analysis (PCA) helps by reducing the data's dimensions while keeping the most important spectral details. This makes CNN computations more efficient and easier to handle.

The HSI cube is partitioned into small overlapping 3D patches, the truth labels of which are determined by the label of the centring pixel. This process involves creating neighbouring patches$N_p \epsilon \mathbb{R}^{(\omega \times \omega \times k)}$ where k is the number of PCA component with a spatial window $(w \times w)$ centered at the spatial location (x, y). For each n patches,$(M-(\omega+1)) \times (L-(\omega+1))$, the dimensions cover the width and height from $(x-(\omega-1)/2)$ to $(x+(\omega-1)/2)$and (y−(ω −1)/2) to (y + $(\omega-1)/2)$.

Hybrid CNN Model

The hybrid CNN model combines 3D and 2D convolutions to leverage the advantages of both types of networks. Initially, the HSI data undergoes 3D convolution to capture joint spatial-spectral features. A 3D-CNN is used to extract spatial-spectral features from the HSI cube. The 3D convolution operation can be mathematically represented as:

$$D_{i,j,k}^{u,v} = ReLu\left(\sum_{\rho=1}^{s_{u-1}} \sum_{\pi=-\gamma}^{\gamma} \sum_{\lambda=-n}^{n} \sum_{\omega=-\varepsilon}^{\varepsilon} Q_{u,v,p}^{\pi,\lambda,\omega} \times D_{(u-1),\rho}^{(i=\gamma)(j+n)(k+\varepsilon)} + b_{u,v}\right) \quad \text{.............. [1]}$$

where $ReLu$ is the activation function, $b_{u,v}$ represents the bias, Q is the depth of the kernel, and D is the feature map. Subsequently, the data is reshaped and passed through 2D convolution layers to enhance spatial feature extraction. The 2D-CNN processes the output from the 3D-CNN to refine the spatial features further. The 2D convolution operation is defined as:

$$D_{i,j}^{u,v} = ReLu\left(\sum_{\rho=1}^{s_{u-1}} \sum_{\pi=-\gamma}^{\gamma} \sum_{\lambda=-n}^{n} Q_{u,v,p}^{\pi,\lambda} \times D_{(u-1),\rho}^{(i=\gamma)(j+n)} + b_{u,v}\right) \quad \text{.............................. [2]}$$

where $D_{i,j}^{u,v}$ is the final output feature map and the parameters are like those used in the 3D convolution equation. The implemented Hybrid architecture with HIS cube size 9 x 9 x 9 is shown in same as (20).

Hybrid Inception Network

Google's Inception network revolutionised convolutional neural networks (CNNs) by introducing the concept of "inception modules"(11). These modules allow the network to capture numerous features at the same time by applying different convolutional filters (e.g., 1x1, 3x3, and 5x5) within a single layer. This architecture increases the network's robustness and efficiency by combining the outputs of various filters along the depth axis. Furthermore, 1x1 convolutions are used within the Inception modules to minimise the dimensionality of the feature maps before applying larger convolutions, which greatly reduces processing costs and the number of parameters while retaining crucial information. The Inception module's parallel nature greatly reduces the computational complexity and memory utilisation concerns faced by traditional CNN models.

To utilise spectral and spatial data through a hybrid method, the suggested Hybrid Inception (3D-2D) model for bloodstain classification is carefully built (Figure 1). The three primary convolutional blocks that make up the design convolve through a succession of 3D convolutions with various filter sizes to collect a variety of spectral-spatial information. The blocks perform 3D convolutional layers with kernel sizes of (1, 1, 1), (3, 3, 3), and (5, 5, 5) to extract complex features and gradually reduce dimension. After the 3D output is flattened into a 2D structure, more 2D convolutions take place for improved feature extraction, followed by max pooling.

Specifically, each block performs a parallel processing operation with its 3D convolutional layers. The 3D CNN outputs are reshaped for 2D CNN with a last temporal 1 × 1 convolution, then max pooling and a sequence of 2D convolutions with growing filter sizes: 32, and 64. Each block allows parallelism in handling computation at different scales of spectral and spatial information, hence can give rich and flexible representation.

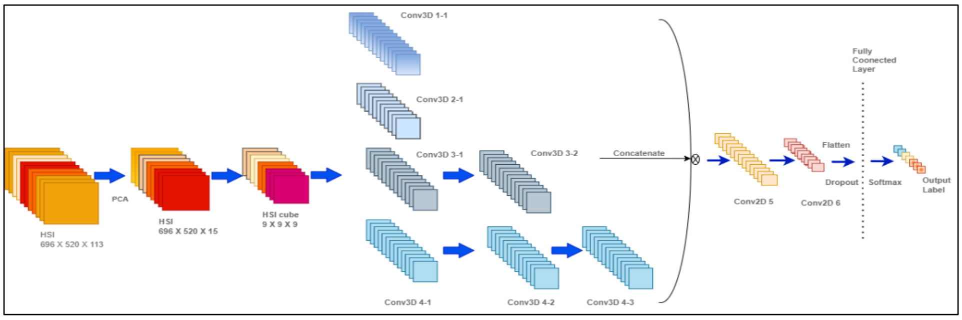

Figure 1: Architectural Depiction of Proposed Hybrid Inception Network

The use of several different kernel sizes from parallel branches offers the network elasticity, allowing it to efficiently deal with unpredictability from hyperspectral data in feature extraction that a single convolutional pathway would otherwise overlook. Reshaping, in combination with 2D convolutions at each block, decreases dimensions and refines features, allowing the model to be computationally economical while retaining crucial information. After processing, the outputs of each convolutional block are concatenated to combine the various features collected from other scales. his is subsequently transmitted through another 2D convolutional layer. The model flattens the feature maps and then moves forward to dense layers for regularization. Finally, a dense output layer classifies the input into one of the seven classes using a softmax activation function. This approach incorporates 3D and 2D convolutions into parallel branch architecture in the 3D-2D Inception model, resulting in a powerful ability to capture full spectral-spatial correlations in hyperspectral data for complex classification tasks in HIS classification.

Table 1: Detail of the Implemented and Modified 2D Inception Network Architecture

Layer	Kernel Size	Parameters
Conv2D 1-1	(1, 1, 8)	128
Conv2D 2-1	(3, 3, 16)	2176
Conv2D 3-1	(1, 1, 8)	128
Conv2D 3-2	(3, 3,16)	1168
Conv2D 4-1	(1, 1, 8)	128
Conv2D 4-2	(3, 3, 16)	1168

Conv2D 4-3	(5, 5, 32)	12832
Concatenate	-	0
Conv2D 5	(3, 3, 32)	20768
Conv2D 6	(3, 3, 64)	18496
Flatten	-	0
Dropout	-	0
Dense	-	51850
Total trainable Parameters	-	87842

Table 2: Detail of the Implemented and Modified 3D Inception Network Architecture

Layer	**Kernel Size**	**Parameters**
Conv3D 1-1	(1, 1, 1, 8)	16
Conv3D 2-1	(3, 3, 3, 16)	448
Conv3D 3-1	(1, 1, 1, 8)	16
Conv3D 3-2	(3, 3, 3, 16)	3472
Conv3D 4-1	(1, 1, 1, 8)	16
Conv3D 4-2	(3, 3, 3, 16)	3472
Conv3D 4-3	(5, 5, 5, 32)	64032
Concatenate	-	0
Conv3D 5	(3, 3, 3, 32)	62240
Conv3D 6	(3, 3, 3, 64)	55360
Flatten	-	0
Dropout	-	0
Dense	-	544327
Total trainable Parameters	-	732,871

Table 3: Details of the Proposed Hybrid Inception Network Architecture

Layer	**Kernel Size**	**Parameters**
Conv3D 1-1	(1, 1, 1, 8)	16
Conv3D 2-1	(3, 3, 3, 16)	448
Conv3D 3-1	(1, 1, 1, 8)	16
Conv3D 3-2	(3, 3, 3, 16)	3472
Conv3D 4-1	(1, 1, 1, 8)	16
Conv3D 4-2	(3, 3, 3, 16)	3472
Conv3D 4-3	(5, 5, 5, 32)	64032
Concatenate	-	0
Reshape	-	-
Conv2D 5	(3, 3, 32)	0
Conv2D 6	(3, 3, 64)	311392
Flatten	-	18496
Dropout	-	0
Dense	-	0
Total trainable Parameters	-	437,627

Our hybrid-inception network uses gradient descent (backpropagation) to train its parameters. Moreover, dropout was implemented with the fully connected layer. The three suggested inception architectures differ considerably in the total amount of trainable parameters, which suggests their different ability to deal with complexity with different model tannable time and feature extraction capacities. The first architecture, a purely 2D convolutional model, as shown in Table 1, has the fewest trainable parameters (87,842), making it relatively lightweight and faster to train but with limited representational power. The second design, a purely 3D convolutional model, given in Table 2, contains a large number of trainable parameters (732,871), indicating a more complex model capable of capturing spatiotemporal patterns in the data, but at the expense of higher computational requirements.

Table 3 shows the third design, a hybrid inception model, which balances the two with 437,627 trainable parameters. The usage of a 3D CNN and a 2D CNN hybrid structure demonstrates that it makes better use of both spatial and spectral data than the strictly 2D model while using fewer resources. This change in parameter count demonstrates the trade-offs between model complexity, computational cost, and performance in HSI classification tasks.

Dataset Description and Experimental Design

The HSI dataset utilized in this research was initially created and reviewed (21). Released under an open-access policy, the dataset encompasses multiple detection scenarios with varying levels of complexity. Hyperspectral data were captured using a Surface Optics SOC710 camera, which operates within the VNIR range of 377–1046 nm. The resulting images have a resolution of 696 × 520 pixels, with 128 spectral bands and a 12-bit dynamic range. The dataset was generated in a controlled laboratory environment, simulating a mock crime scene. Figure 2A illustrates the laboratory setup, including target annotations, documentation, and 14 HSI files (each approximately 180 MB) in ENVI format. 'Scene E' is a subset of the generated mock-up scene, featuring various blood-like traces on eight distinct backgrounds, including fabric, wood, plastic, and metal, some with crimson textures. After noise band removal, the image dimensions are 696 × 520 × 113. These images consist of a sequence of spectral stripes. These images consist of a sequence of spectral stripes. Figure 2B illustrates the presence of substances resembling blood traces, such as tomato concentrate, ketchup, poster paint, acrylic paint, manufactured blood, and unidentified blood. Additionally, their spectral signatures are provided in Figure 3.

The dataset was randomly split into training (80%), validation (10%), and test (10%) samples, as detailed in Table 4. Convolutional network hyperparameters were fine-tuned based on prior experience and experimental findings. For all experiments, the Adam optimizer was used with a learning rate of 1e-3 and a decay term of 1e-6. Optimal network settings were determined through trial and error and refined using a mini-batch-based backpropagation method. Training was conducted for 100 epochs with a mini-batch size of 32.

Table 4: Summary of Class Distribution in the 'Scene E(1)' Bloodstain Dataset

Class	**Training**	**Validation**	**Test**
Blood	296	296	2372
Ketchup	584	584	4675
Artificial Blood	641	642	5133
Poster Paint	662	663	5300
Tomato Concentrate	393	394	3148
Acrylic Paint	802	802	6417
Total	3378	3378	27048

Multiple metrics were used to evaluate the performance of the tested models, including execution time, average accuracy (AA), overall accuracy (OA), and the Kappa coefficient (K × 100). The Kappa coefficient quantifies the agreement between predicted and actual classifications while accounting for chance, providing a robust measure of classification accuracy. Overall accuracy (OA) represents the proportion of correctly classified samples across the entire dataset, serving as a key performance indicator. Average accuracy (AA) calculates the mean accuracy across all classes, ensuring equal weighting and highlighting the model's ability to handle class imbalances. Execution time measures computational efficiency, indicating the time required for classification and the trade-off between accuracy and computational cost.

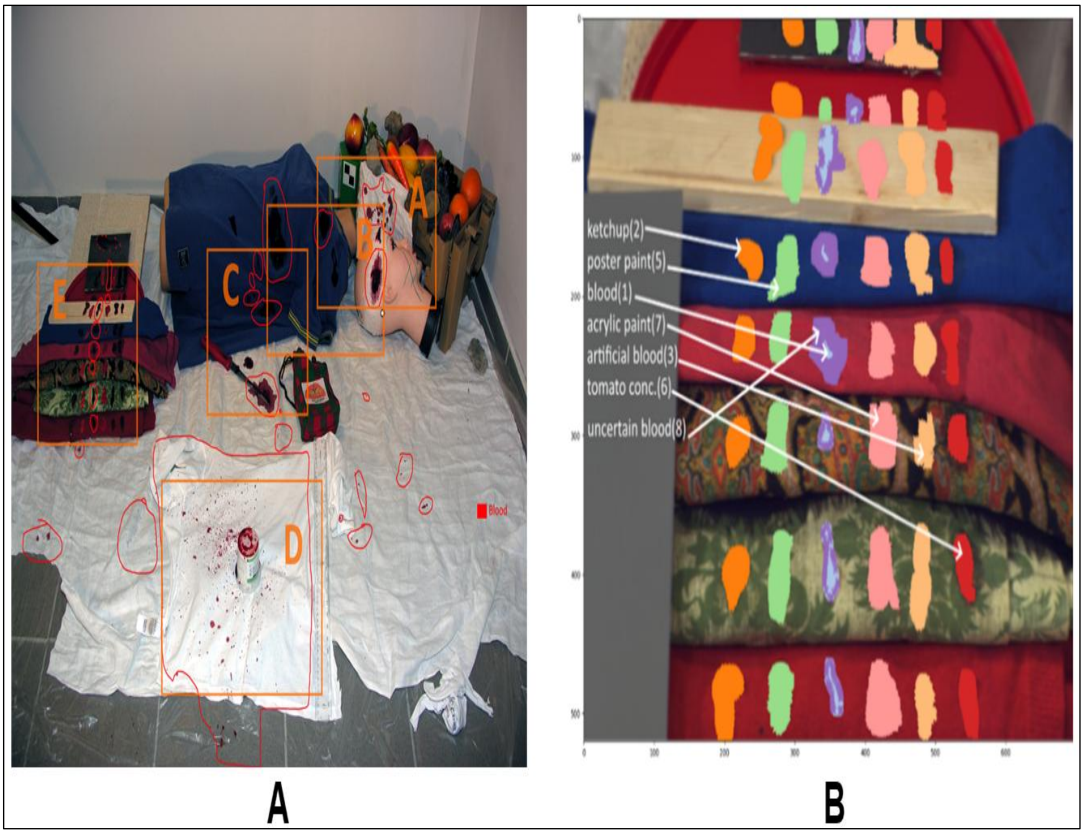

Figure 2: Illustration of the Dataset, (A) The Mock-Up Crime Scene Setup (With Locations of Images A-E), (B) Overview of the E 'Frame' Scene

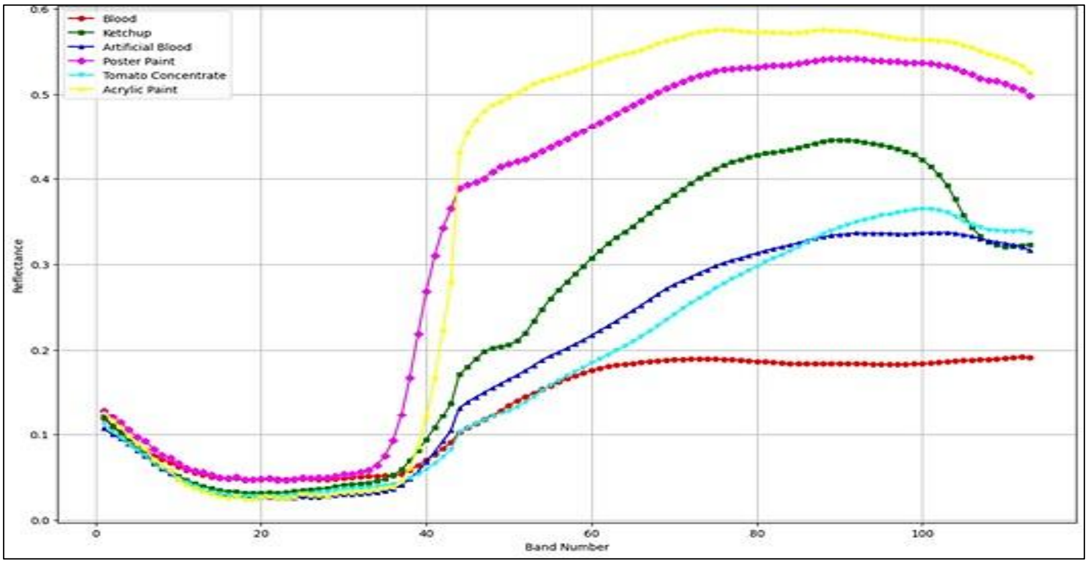

Figure 3: Spectral Signatures of Experimental Samples, Including Blood, Ketchup, Artificial Blood, Poster Paint, Tomato Concentrate, and Acrylic Paint, in 'Scene E(1)'

The Bloodstain dataset image E(1) was processed using PCA to reduce dimensionality, resulting in 9 × 9 × 9 × 15. image cubes as input for the network. Table 5 compares the classification performance of the three proposed networks—2D Inception Network, 3D Inception Network, and 3D-2D Hybrid Inception Network—with three commonly used methods: 2D CNN, 3D CNN, and Hybrid CNN. Additionally, classification accuracies were visually represented. Figure 4 depicts the ground truth maps generated after evaluating the proposed Inception-based models on image E(1) from the bloodstain dataset.

Results and Discussion

The **Table 5** shows a comparison of all six implemented network architectures results: 2DCNN, 3DCNN, Hybrid CNN, 2DIN, 3DIN, and Hybrid Inception. Each network's performance is assessed across various material classes, including blood, ketchup, artificial blood, poster paint, tomato concentrate, and acrylic paint on eight different backgrounds. Notably, the Hybrid Inception network outperforms most categories, suggesting its effectiveness in classifying HSI. Where Hybrid CNN also shows promising classifying numbers. The Hybrid CNN and Hybrid Inception models perform exceptionally well when class-wise accuracy is examined; they receive perfect scores (100%) for classes like Poster Paint and Blood. It demonstrates their flawless ability to classify these substances precisely. The 2DCNN and 3DCNN models, on the other hand, have much lower accuracy for some classes, such as Tomato Concentrate, where the 2DCNN only gets 83.50% and the 3DCNN gets 87.80%. The Hybrid CNN and Inception models have far longer execution times despite their great accuracy. The 2DCNN completes tasks in 87.25 seconds, whereas the 3DIN model takes 688.12 seconds, indicating a trade-off between speed and accuracy with the increase in number of trainable parameters.

Table 5: Comparisons of Classification Accuracies among Different Methods

Class	2DCNN	3DCNN	Hybrid CNN	2D Inception	3D Inception	Hybrid Inception
Blood	92.40	97.20	100	97.20	99.50	99.50
Ketchup	95.90	98.80	99.80	98.80	99.00	99.80
Artificial Blood	93.70	92.20	99.10	90.70	92.00	99.30
Poster Paint	99.40	99.80	100	99.90	99.90	99.90
Tomato Concentrate	83.50	87.80	92.60	90.40	93.90	95.00
Acrylic Paint	98.40	99.90	99.70	99.00	98.80	100
OA(%)	95.01	96.59	98.85	96.00	97.28	99.18
AA(%)	93.87	95.96	98.52	96.00	97.21	98.90
Kappa	93.88	95.83	98.60	95.10	96.68	98.95
Executions Time (s)	87.25	121.12	132.00	208.00	688.12	485.00

The hybrid inception network exhibits a robust and reliable result in HSI classification, shown by its high overall accuracy (99.18%), average accuracy (98.90%), and Kappa coefficient (98.95). This model is the finest option for applications where precision is crucial because it regularly performs better than others. The 2D CNN, on the other hand, has the quickest execution time but shows worse performance metrics, indicating that it would be better suited for situations when speed is more important than accuracy. These results emphasize the importance of selecting the best model for a given set of application requirements, weighing classification accuracy against execution time and need of resources to get the best outcomes.

The classification maps in Figure 3 show minimal qualitative differences between the deep learning models. However, Table 5 provides quantitative evidence that the 3D-2D Hybrid Inception Network achieved the highest performance. While 3D Inception Networks outperformed 2D-CNN and 3D-CNN, the Hybrid Inception Networks and Hybrid CNN demonstrated superior accuracy. A closer analysis of Table 5 confirms this trend. Additionally, the classification map for the Hybrid Inception Network closely resembles the ground truth map, as shown in Figure 4.

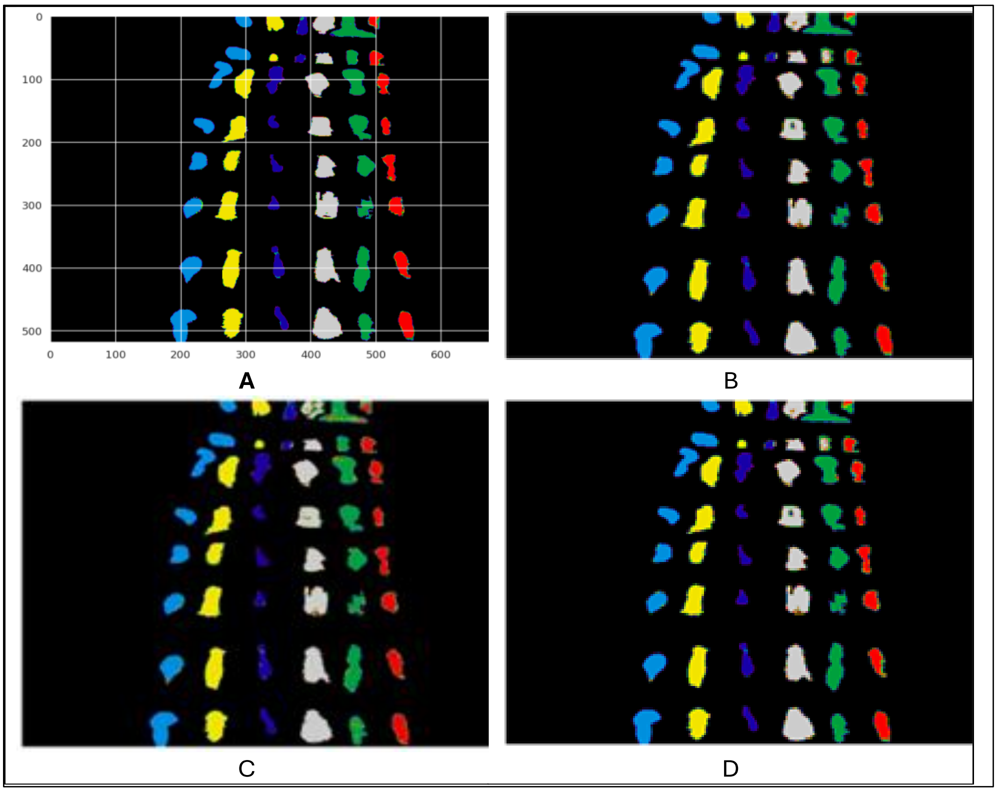

Figure 4: Classification Maps for (A) Ground Truth, (B) 2D Inception (C) 3D Inception (D) Hybrid Inception Model

Conclusion

The methods used in this research are non-destructive, effective, and rapid. We introduced a 3D-2D hybrid inception network for spectral-spatial joint feature extraction and classification to increase the classification accuracy of HSIC. With only a few training examples, the proposed 3D–2D hybrid inception network achieves high classification accuracy. With the fine tuning and updating of the models, we can also have satisfactory classification rates for hybrid CNN and 3D inception networks. The experimental results also showed that the proposed methodologies have the potential to improve blood classification using HSI technology for real-world crime detection. Possible future research directions include using various time-delayed HSIs to identify bloodstains that degrade over time. Additionally, the developed model can be utilised using transfer learning to identify other body fluids at crime scenes.

Abbreviations

None.

Acknowledgement

None.

Author Contributions

Tejaskumar B Sheth: Conceived the study, Methodology, Implemented the YOLOv4 model, Analysed data, Write, Milind S Shah: Data Collection, Model Development, Review, Suhas H Patel: Literature review, and helped to edit the manuscript.

Conflict of Interest

The authors declare no conflict of interest on this work.

Ethics Approval

Not applicable.

Funding

None.

References

1. Sijen T, Harbison S. On the Identification of Body Fluids and Tissues: A Crucial Link in the Investigation and Solution of Crime. Genes . 2021 Oct 28;12(11):1728.
2. Harbison S, Fleming R. Forensic body fluid identification: state of the art. Research and Reports in Forensic Medical Science . 2016 Feb;2016(6):11.
3. Schalik R, Illes M. A Review of Spectroscopic Methods Applied to Bloodstain Pattern Analysis. Journal of

Multidisciplinary Research at Trent. 2019;2(1):90–104.
4. Majda A, Wietecha-Posłuszny R, Mendys A, Wójtowicz A, Łydżba-Kopczyńska B. Hyperspectral imaging and multivariate analysis in the dried blood spots investigations. Applied Physics A: Materials Science and Processing . 2018;124(4):1–8.
5. Romaszewski M, Głomb P, Sochan A, Cholewa M. A dataset for evaluating blood detection in hyperspectral images. Forensic science international. 2021 Mar 24;320:110701.
6. Guerri MF, Distante C, Spagnolo P, Bougourzi F, Taleb-Ahmed A. Deep Learning Techniques for Hyperspectral Image Analysis in Agriculture: A Review. ISPRS Open Journal of Photogrammetry and Remote Sensing . 2023 Apr 26;12:1–30.
7. Mohan A, Venkatesan M. HybridCNN based hyperspectral image classification using multiscale spatiospectral features. Infrared Physics & Technology. 2020 Aug 1;108:103326.
8. Roy SK, Deria A, Hong D, Ahmad M, Plaza A, Chanussot J. Hyperspectral and LiDAR data classification using joint CNNs and morphological feature learning. IEEE Transactions on Geoscience and Remote Sensing. 2022 May 23;60:1-6.
9. Iyer P, Sriram A, Lal S. Deep learning ensemble method for classification of satellite hyperspectral images. Remote Sensing Applications: Society and Environment. 2021 Aug 1;23:100580.
10. Wang X, Liu J, Chi W, Wang W, Ni Y. Advances in Hyperspectral Image Classification Methods with Small Samples: A Review. Remote Sensing . 2023 Jul 30;15(15):3795.
11. Szegedy C, Liu W, Jia Y, Sermanet P, Reed S, Anguelov D, et al. Going deeper with convolutions. In: Proceedings of the IEEE Computer Society Conference on Computer Vision and Pattern Recognition . IEEE. 2015:1–9. http://ieeexplore.ieee.org/document/7298594/
12. Webb JL, Creamer JI, Quickenden TI. A comparison of the presumptive luminol test for blood with four non-chemiluminescent forensic techniques. Luminescence . 2006 Jul 27;21(4):214–20.
13. Virkler K, Lednev IK. Analysis of body fluids for forensic purposes: From laboratory testing to non-destructive rapid confirmatory identification at a crime scene. Forensic Science International . 2009 Jul 1;188(1–3):1–17.
14. Finnis J, Lewis J, Davidson A. Comparison of methods for visualizing blood on dark surfaces. Science and Justice . 2013;53(2):178–86.
15. Zhao Y, Hu N, Wang Y, Liu Y, Li X, Wang J. The application of near-infrared reflectance hyperspectral imaging for the detection and extraction of bloodstains. Cluster Computing . 2019;22:8453–61.
16. Khan MJ, Khan HS, Yousaf A, Khurshid K, Abbas A. Modern Trends in Hyperspectral Image Analysis: A Review. IEEE Access. 2018;6:14118–29.
17. Bhatt PV, Rawtani D. Spectroscopic Analysis Techniques in Forensic Science. In: Modern Forensic Tools and Devices: Trends in Criminal Investigation . 2023:149–97. https://onlinelibrary.wiley.com/doi/10.1002/9781119763406.ch8
18. Cuttaia C, Di Stefano B, Sorçaburu Ciglieri S, Vetrini R, Previderè C, Fattorini P. Immunochromatographic Detection of Human Blood: A Forensic Review. Separations. 2024;11(3):1–13.
19. Mariotti K de C, Ortiz RS, Ferrão MF. Hyperspectral imaging in forensic science: An overview of major application areas. Science and Justice. Forensic Science Society; 2023;6:387–95.
20. Butt MHF, Ayaz H, Ahmad M, Li JP, Kuleev R. A Fast and Compact Hybrid CNN for Hyperspectral Imaging-based Bloodstain Classification. 2022 IEEE Congress on Evolutionary Computation, CEC 2022 - Conference Proceedings . 2022 :1–8. https://ieeexplore.ieee.org/document/9870277/
21. Książek K, Romaszewski M, Głomb P, Grabowski B, Cholewa M. Blood Stain Classification with Hyperspectral Imaging and Deep Neural Networks. Sensors . 2020 Nov 21;20(22):6666.